Raman scattering and supercontinuum generation in high-index doped silica chip waveguides

Charbel Khallouf, Van Thuy Hoang, Gil Fanjoux, Brent Little, Sait Chu, Dave Moss, Roberto Morandotti, John Dudley, Benjamin Wetzel, Thibaut Sylvestre

Raman scattering and supercontinuum generation in high-index doped silica chip waveguides

C. Khallouf[1], V. T. Hoang[2], G. Fanjoux[1], B. Little[3], S. T. Chu[4], D. J. Moss[5], R. Morandotti[6], J. M. Dudley[1], B. Wetzel[2], and T. Sylvestre[1]

[1]Institut FEMTO-ST, CNRS-Université de Franche-Comté, 25030 Besançon, France
[2]XLIM Research Institute, CNRS UMR 7252, Université de Limoges, 87060 Limoges, France
[3]QXP Technologies Inc., Xi'an, China
[4]Department of Physics, City University of Hong Kong, Tat Chee Avenue, Hong Kong, China
[5]Optical Sciences Centre, Swinburne University of Technology, Hawthorn, Victoria, Australia
[6]INRS-EMT, 1650 Boulevard Lionel-Boulet, Varennes, J3X 1S2, Québec, Canada

ABSTRACT

We present a comprehensive investigation of Raman scattering (RS) and supercontinuum (SC) generation in high-index doped silica glass integrated optical waveguides under diverse femtosecond pumping wavelengths and input polarization states. We first report the observation based on a confocal Raman microscope of new Raman peaks different from fused silica at 48 THz and 75 THz, respectively. We then demonstrate broadband supercontinuum generation from 700 nm to 2500 nm when pumping into the anomalous dispersion regime at 1200 nm, 1300 nm, and 1550 nm, respectively. Conversely, narrower SC spectra were generated when pumping in the normal dispersion regime at 1000 nm of self-phase modulation and optical wave breakup. A good agreement is found with numerical simulations of a nonlinear Schrödinger equation including the new Raman response. We also study the impact of the TE/TM polarization modes of the integrated waveguide on SC generation.

Keywords: Supercontinuum generation, Raman scattering, integrated chip waveguides, nonlinear optics, high index glasses

1. INTRODUCTION

Recent years have seen tremendous advances in improving supercontinuum (SC) light generation in diverse transparent nonlinear materials and waveguides.[1,2] This is because SC generation (SC) converts laser light, typically from a pulsed laser, into a wide continuous optical spectrum ranging from the visible to the infrared regions, making these novel sources useful in a plethora of applications. Important applications of broadband SC sources include optical coherence tomography (OCT), fluorescence imaging, optical sensing, absorption spectroscopy, and optical frequency comb metrology.[3–9] While SC light has been the subject of extensive research in specialty optical fibers for more than thirty years, today research is now focused on the development of compact, low-threshold SC sources based on integrated photonic chips. Indeed, the recent technological advances in the design and fabrication of highly nonlinear integrated photonic chip waveguides are currently driving new research on nonlinear effects and SC generation in various materials, and yet unexplored regions of the electromagnetic spectrum such as mid-infrared. SC generation has already been demonstrated and characterized in many integrated and dispersion-engineered photonic integrated circuits based on glasses or wide band-gap semiconductors, such as silica (SiO_2),[10] silicon nitride (SiN),[11–13] high index doped silica glass (HDSG),[14] silicon germanium (SiGe),[15,16] titanium dioxide (TiO_2),[17] chalcogenide glass (As_2S_3),[18] AiN,[19] GaAs,[20] LNOI.[21] A complete review of the recent progress on chip-based SC sources can be found in Reference.[22] Among nonlinear materials, high-index doped silica glass (HDSG) is very promising because it has several advantages including a wide transparency window, a nonlinearity greater than pure fused silica, no free carrier or nonlinear absorption.[14] Although SC generation in an HDSG waveguide has already been investigated in the past, the role of Raman scattering,

Further authors information: CK, TS or BW
E-mails: charbel.khallouf@femto-st.fr, thibaut.sylvestre@univ-fcomte.fr, benjamin.wetzel@unilim.fr

normal or anomalous dispersion pumping regimes, and polarization effects on SC generation hitherto remains elusive.

We provide in this paper new results of stimulated Raman scattering (SRS) and supercontinuum (SC) generation in a 50-cm long spiral HDSG integrated waveguide under various pumping wavelengths and input polarization states. We first report the observation of two new Raman peaks, other than the fused silica's peak, at 48 THz and 75 THz, respectively, using a confocal Raman micro-spectrometer at 532 nm. It is further shown, both numerically and experimentally, that these new peaks have little impact on SC generation under femtosecond pulse excitation. Nearly flat SCs were generated from 700 nm until 2500 nm, when pumping the waveguide in the anomalous dispersion regime (at 1200 nm, 1300 nm, and 1550 nm), by soliton self-frequency shift (SSFS) and dispersive wave (DW) generation. Conversely, narrower SC was obtained when pumping the waveguide in the normal dispersion regime (at 1000 nm) due to self-phase modulation (SPM), optical wave breaking (OWB), and the new Raman peaks. We further investigated the impact of TE/TM pump polarization modes on SC generation and found a good agreement with numerical simulations of the modified nonlinear Schrödinger equation.

2. HIGH-INDEX DOPED SILICA CHIP WAVEGUIDE

Since early developments of high index, low-loss, CMOS compatible doped silica glass material,[23] significant improvements were made achieving ultra-low loss (<0.1 dB/cm) highly doped silica glass waveguide now fabricated by QXP Technologies Inc. Figure 1(a) shows the cross-section on the QXP-chip waveguide. The core's size is of 1.5 $\mu m \times 1.52\ \mu m$ integrated into plasma-enhanced chemical vapor deposition (PECVD) silica (SiO_2), and deposited on SiO_2 thermal oxide, all deposited on a Silicon wafer. The chip is made up of 20 reversible input/output waveguides, all connected to 25cm-long fiber pigtails, thus facilitating the coupling and extraction of guided light. For SC generation, we experimentally investigated the 50-cm long HDSG waveguide, which includes 2 spirals of 25 cm long each. The total insertion loss of this 50-cm long waveguide has been measured to be 8.9 dB at =1550 nm by using a high-resolution optical time domain reflectometer (OBR 4600 Luna Tech.). The OBR trace is shown in Fig. 1(b) with a sampling resolution of 20 µm, and the linear loss has been estimated to be as low as 0.1 dB/cm.[24]

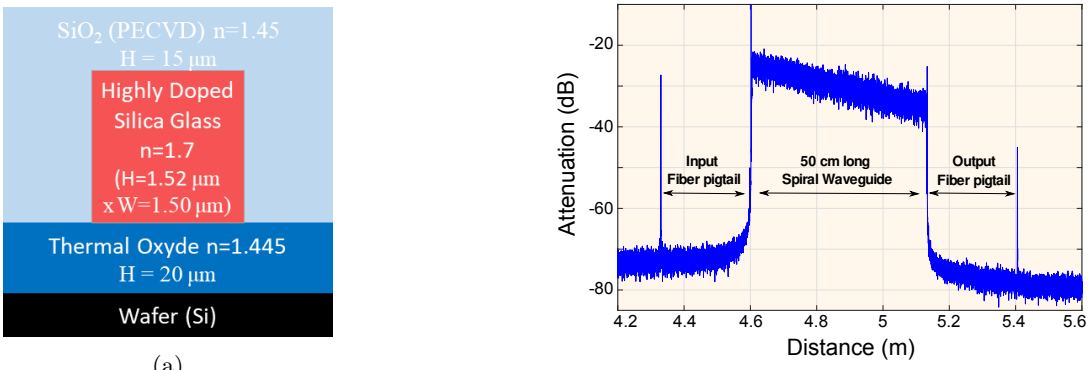

(a) (b)

Figure 1: (a) Cross-section of the highly doped silica glass waveguide (HDSG) from QXP technologies; (b): OBR Trace showing the losses of the 50-cm long waveguide and of the fiber pigtails at telecom wavelength λ=1550 nm.

3. DISPERSION AND EFFECTIVE MODAL AREA

Based on the cross-section of the integrated waveguide, we first calculated the effective refractive indices of the fundamental modes, as well as the different dispersion and non-linearity parameters. A finite element method (FEM) based software was used to solve these wavelength-dependent parameters by scanning from 700 nm to 3000 nm. The results are provided in Figure 2, which shows the group-velocity dispersion D in (a) and the

effective mode area in (b) of the two TE/TM fundamental modes in blue and red, respectively. The dispersion profiles for both TE/TM modes exhibit three zero-dispersion wavelengths (ZDW) near 1000 nm, 1800 nm and 2300 nm, respectively. The birefringence of the waveguide has been estimated below 10^{-4} at 1550 nm.

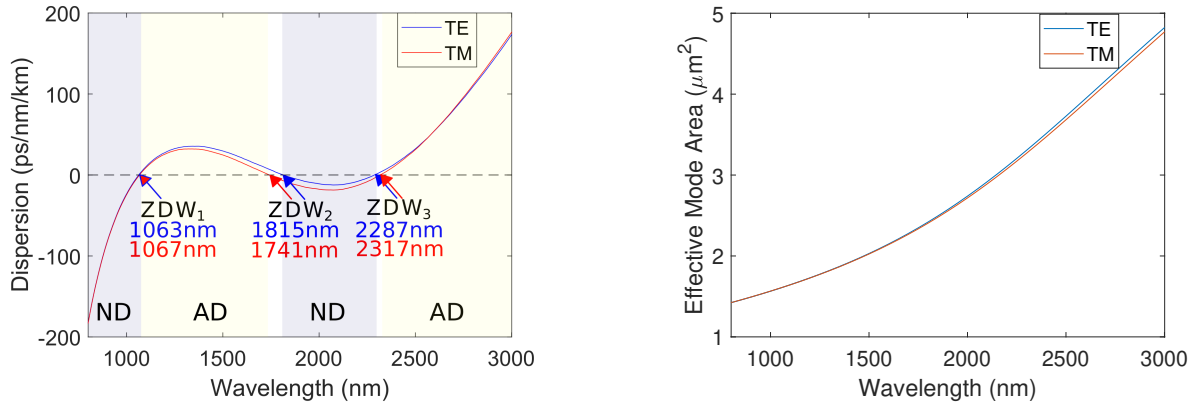

(a) (b)

Figure 2: (a): Group Velocity Dispersion D of the QXP-chip waveguide with the zero-dispersion wavelengths (ZDW) of the 2 fundamental TE and TM modes in blue and red, respectively, ND/AD Normal/Anomalous Dispersion; (b): Effective Modal Area A_{eff} of the two fundamental TE and TM modes versus wavelength.

According to Fig. 2(a), pumping wavelengths will cover both dispersion regimes. So when pumping at 1000 nm, i.e, in the normal dispersion regime, one can expect to have an SC generation by SPM and OWB, while pumping at 1200 nm, 1300 nm, 1550 nm, i.e in the anomalous dispersion regime one can expect to have a broader SC generation by soliton fission, self-frequency shift and dispersive wave generation. Fig. 2(b) also shows that the effective modal area A_{eff} of the two fundamental TE and TM modes strongly varies across wavelength.

4. RAMAN SPECTRUM OF THE HIGH-INDEX DOPED SILICA GLASS

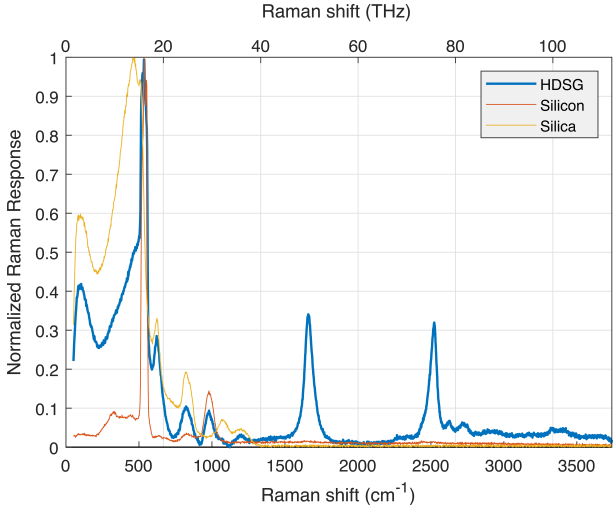

Figure 3: Raman spectra of the integrated HDSG waveguide in blue, of the Silicon in orange, and Silica in yellow.

The Raman spectra presented in Fig. 3 were acquired using a high-resolution confocal Raman microscope (Monovista CRS+), employing a 532 nm continuous doubled Nd:YAG laser beam and a 100x microscope objective. Achieving optimal depth focus was essential to ensure precise targeting of the laser beam onto the highly

doped silica waveguide (HDSG), rather than onto the surrounding silica coatings. The Raman spectra of silica (yellow) and silicon (orange) were obtained by directing the laser beam onto the upper layer of the PECVD SiO_2 layer and the silicon wafer, respectively.

During the focusing process on the HDSG material, Raman scattering from silica originating from the surrounding coatings, as well as from the material itself, along with signals from the silicon wafer, were consistently observed. However, notable are the emergence of two distinct peaks at 1655 cm^{-1} (49.6 THz) and 2515 cm^{-1} (75.4 THz) (refer to Fig. 3). It is noteworthy that a normalization process was employed for clarity purposes in the presented data.

5. EXPERIMENTAL SETUP

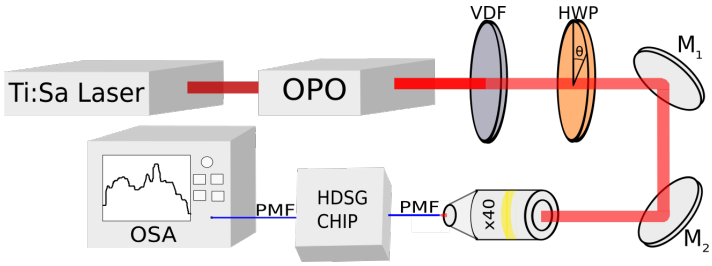

Figure 4: Experimental setup for the SC generation and measurement.

The experimental setup used for generating and measuring SC spectra is shown in Fig. 4. A 200-fs Optical Parametric Oscillator (Chameleon Compact OPO-Vis) served as the pump laser, driven by a Ti-Sapphire mode-locked laser (Chameleon Ultra II) at an 80 MHz repetition rate. The OPO signal is tunable in the range 1-1.6 μm with mean output powers from 230 mW to 1 W, and the idler from 1.7 μm to 4 μm with powers from 250 mW to 50 mW. Control over power and polarization angles θ was achieved through a variable density filter (VDF) and a half-wave plate (HWP), respectively. The signal from the OPO was injected into a standard fiber pigtail through a system of 2 mirrors M_1 and M_2 and an IR focusing objective (x40). The generated SC light was then analyzed using two different spectrometers (Agilent OSA 600-1700 nm with a further nonlinear response between 1700-2000 nm and an FTIR Thorlabs OSA 205C from 1000-5600 nm).

6. EXPERIMENTAL SC RESULTS

As anticipated, the supercontinuum (SC) generated across these various pumping wavelengths arises from soliton self-frequency shift within the anomalous dispersion regime, coupled with dispersive wave generation transitioning into the normal dispersion regime. Notably, when employing a pump wavelength of 1550 nm typical for telecom applications, the resulting SC spectrum spans from 700 nm to well beyond the upper limit of the Agilent Optical Spectrum Analyzer (OSA) at 2000 nm (Fig. 5(a)). Consequently, supplementary measurements utilizing the Thorlabs OSA were necessary (refer to Fig. 5(b)). However, to prevent intensity saturation of the Thorlabs spectrometer, the input power at the entrance of the focusing objective was constrained to 220 mW, corresponding to an output power of 9 mW. Despite this limitation, a discernible SC is evident, extending up to 2500 nm.

Additionally, Fig. 5(a) illustrates a residual idler at 1740 nm from the Optical Parametric Oscillator (OPO). This idler, being weak and unsynchronized with the pump pulse, does not interfere with the SC generation process. For other pumping wavelengths, idler residues extend beyond 2000 nm and do not manifest in the measurements. The SC depicted in Figs. 5(c) and 5(d) ranges from 700-750 nm to 2000 nm, with a notable peak at 700 nm in Fig. 5(c), subject to further investigation in subsequent polarization analyses.

Here, the polarization angle was chosen to maximize SC bandwidth, suggesting compatibility with either the TE mode or TM mode. The spectral dip observed at 1380 nm in Figs. 5 is due to OH^- absorption within the integrated waveguide. Nonetheless, this absorption does not impede SC extension into the infrared spectrum.

Figure 6 illustrates spectral outcomes when pumping at 1000 nm within the normal dispersion regime. As expected, minimal supercontinuum (SC) extension is observed, primarily attributed to self-phase modulation

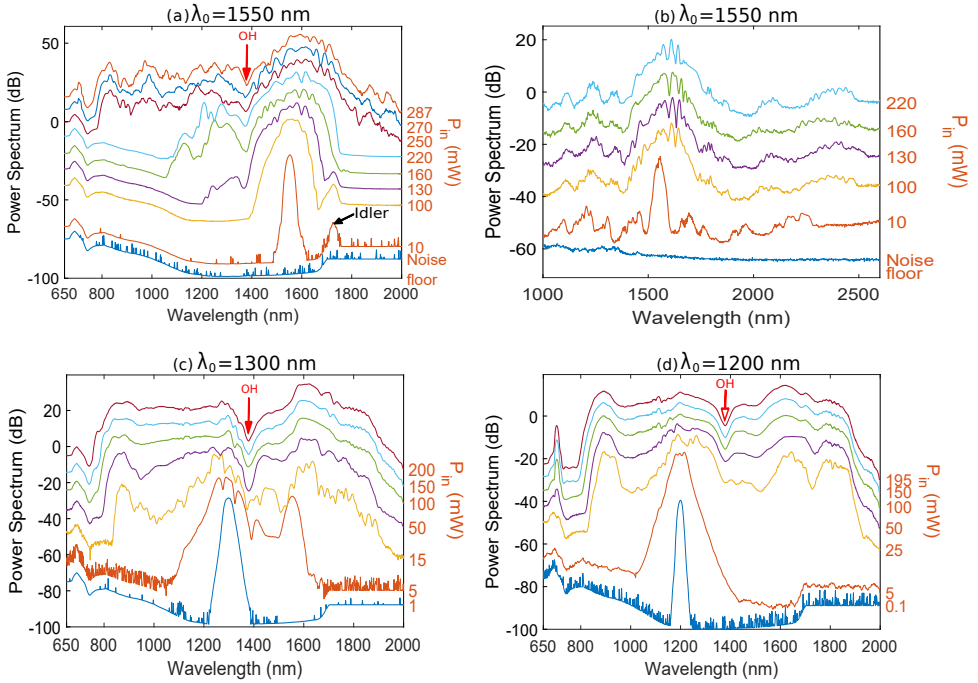

Figure 5: SC spectra in the anomalous dispersion pumping regime for an increasing input mean power measured at the entry of the focusing objective, shown on the right side of the graph for different pumping wavelengths λ_0 (1550nm, 1300nm, and 1200nm); (a),(c),(d) were measured with the Agilent OSA while (b) was measured with the Thorlabs OSA.

(SPM) and optical wave breaking (OWB). At lower pump power levels, the SC exhibits quasi-symmetric spectral broadening, ceasing upon reaching the first zero-dispersion wavelength (ZDW1) near 1065 nm at higher powers. Notably, a distinctive peak emerges near 1150 nm (Fig. 6), characteristic of dispersive wave generation from OWB within the anomalous dispersion regime, a phenomenon previously observed in optical fibers.[25] This observation will be further corroborated through numerical simulations.

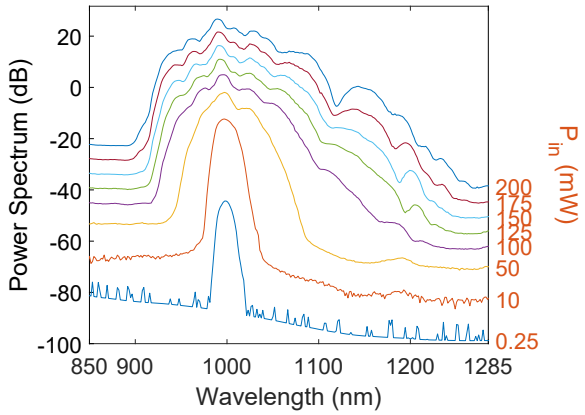

Figure 6: SC spectra in the normal dispersion regime with an increasing input power measured at the entry of the focusing objective, shown on the right side, when pumping at 1000 nm, measured with the Agilent OSA.

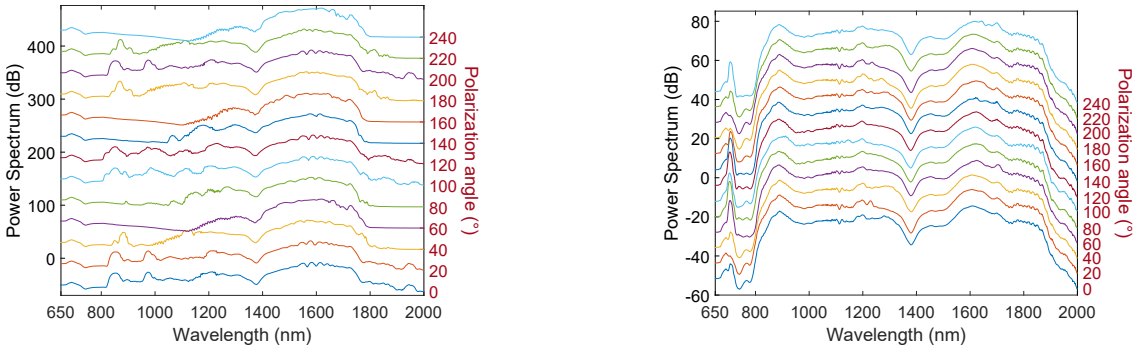

Figure 7: SC generation in the anomalous dispersion regime for different input polarization angles, depicted on the right side of the graph with an input power P_{in} measured at the entry of the focusing objective for a pumping wavelength of (a) 1550 nm with P_{in}= 250 mW ; (b) 1200 nm with P_{in}= 195 mW.

7. EXPERIMENTAL POLARIZATION ANALYSIS

When pumping at 1550 nm, Fig. 7(a) shows a notable dependency of the supercontinuum (SC) generation process on the polarization angle. The SC exhibits a wide spectral spread ranging from 800 nm to 2000 nm for certain polarization angles, whereas for others, it spans from 1150 nm to 1800 nm. Intriguingly, there is an observed angle periodicity of approximately 90°±10°. For instance, SC spectra exhibit similar characteristics at polarization angles of 60°, 160°, and 240°. Conversely, when pumping at 1200 nm, as depicted in Fig. 7(b), the polarization angle demonstrates less influence on the SC generated within the 800-2000 nm range. However, a distinct peak near 700 nm displays strong polarization dependence with a periodicity of 180°.

8. NUMERICAL SIMULATIONS

In our numerical simulations, we used the scalar generalized nonlinear Schrödinger equation (GNLSE) to model the nonlinear pulse propagation within the QXP chip. This equation is expressed in the following reduced form[2]

$$\frac{\partial A}{\partial z} + \frac{\alpha}{2}A - i\sum_{n\geq 2}^{\infty} i^{n+1}\frac{\beta_n}{n!}\frac{\partial^n A}{\partial T^n} = i\gamma \times \left[(1-f_R)|A|^2 A + f_R A\int_0^{+\infty} h_R(T')\,|A(T-T')|^2\,dT'\right], \qquad (1)$$

where A(z,T) is the complex amplitude of the field propagating in the z direction and in the pump velocity time frame T. β_n is the n^{th} derivative of the propagation constants, $h_R(T)$ the delayed temporal Raman response, α the wavelength-dependent propagation loss, and f_R the fractional contribution of the Kerr effect ($f_R = 0.18$, we assume the same value as the standard silica fiber).[26] The nonlinear coefficient $\gamma = 2\pi n_2/(\lambda_0 A_{eff}(\lambda_0))$ with n_2 the nonlinear index of the high index silica glass n_2 =$1.15\times10^{-19} m^2/W$ [27,28] and $A_{eff}(\lambda_0)$ the effective area of the fundamental mode for the pump wavelength λ_0.[26] The nonlinear coefficient was then estimated from the computed modal area plotted in Fig. 2(b). At 1550 nm, $\gamma = 250 W^{-1}km^{-1}$, which represents about 125 times larger than a standard silica fiber (SMF-28).

In our simulations, we averaged the results of 20 pulses under varying input quantum noise conditions, assuming a polarization aligned with the fundamental TE mode. Additionally, we incorporated the dip resulting from OH^- absorption into the simulation. Figures 8(a-d) present the simulation outcomes for different input peak powers (P_0), indicated on the right side of the graph, corresponding to the same four pumping wavelengths (λ_0) utilized in the experimental setup. A quite good agreement is observed between the experimental data shown in Fig. 5 and our simulations.

Specifically, when pumping at 1550 nm, the simulated SC spreads from 700 nm to 2500 nm (Fig. 8(a)). Similarly, for a pump wavelength of 1300 nm, the simulated SC also extends from 750 nm to 2000 nm (Fig. 8(b)).

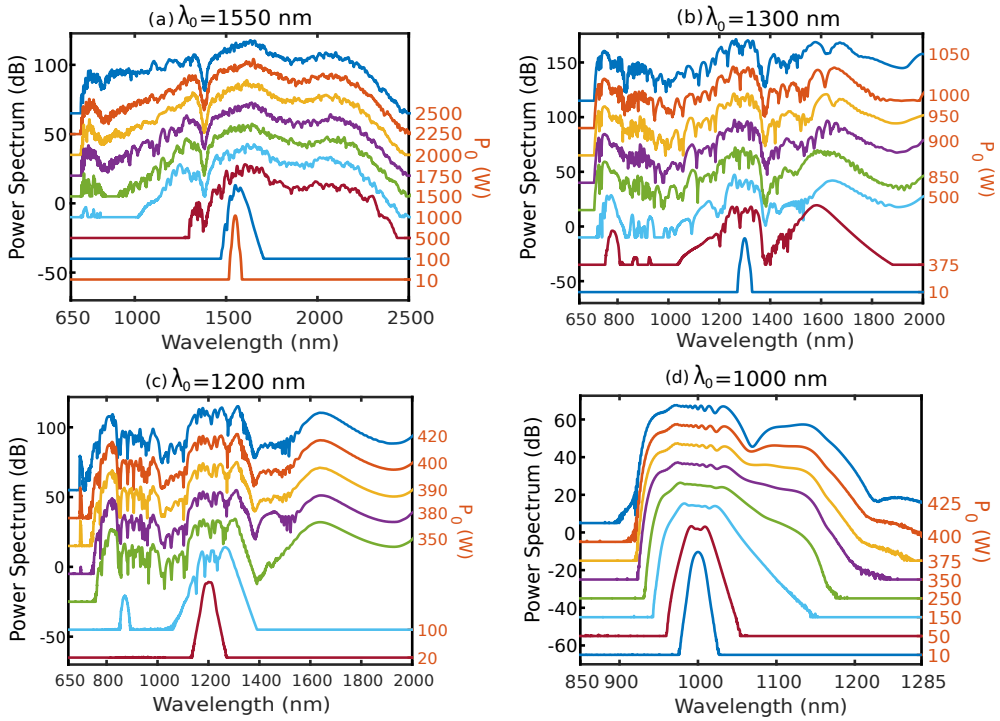

Figure 8: Numerical results: SC generation for different input peak powers P_0 shown on the right side of the graph and for different pumping wavelengths λ_0.

The peak observed experimentally at 700 nm when pumping at 1200 nm is also replicated in the simulations, with the SC spanning from 700 nm to 2000 nm (Fig. 8(c)). This peak actually relies on a four-wave mixing (FWM) interaction within the SC.

Furthermore, when pumping at 1000 nm, we observe consistent behaviors between simulations and experiments (Fig. 6), particularly the symmetry in the spectra, which breaks upon reaching the first zero-dispersion wavelength (ZDW) (Fig. 8(d)). An important aspect of the agreement between experiments and TE simulations is that the measurements were predominantly conducted along one of the TE/TM axes. This alignment is justified by the selection of the polarization angle, which aimed to maximize the spectral broadening, noting that SCs generated in the fundamental TM mode exhibited nearly identical characteristics to those in the fundamental TE mode.

Nevertheless, a slight difference between experiments and simulations is noticeable, primarily attributed to wavelength-dependent losses, which were not fully characterized except at the telecom wavelength of 1550 nm (0.1 dB/cm), and also due to variations in the responses and sensitivities of the two optical spectrum analyzers (OSAs).

9. CONCLUSION AND DISCUSSION

In conclusion, our study focused on investigating supercontinuum (SC) generation within a 50 cm long highly doped silica glass spiral waveguide under varying dispersion regimes and polarization angles. Notably, the broadest SC spectrum was achieved when pumping at 1550 nm, spanning from 700 nm to 2500 nm. Our observations revealed a high sensitivity of the SC to polarization angle at the 1550 nm pump wavelength, whereas this sensitivity decreased for smaller pump wavelengths.

Given their nonlinear optical properties, straightforward manufacturing process and compatibility with fiber optics technologies, these QXP glass-based integrated photonic waveguides hold significant promise for the development of compact and low pulse energy supercontinuum sources based on compact fs fiber lasers. Such on-chip

SC sources could potentially find applications across various fields requiring broad spectral coverage, including spectroscopy, telecommunications, and biomedical imaging, among others.

10. ACKNOWLEDGMENTS

This project has received funding from the Agence Nationale de la Recherche (ANR) (ANR-16-CE24-0010, ANR-15-IDEX-0003, EUR EIPHI Graduate School ANR-17-EURE-0002), the Bourgogne Franche-Comté Region, the Horizon Europe Framework Programme (VISUAL Action 101135904) and the European Research Council (ERC) under the European Union's Horizon 2020 research and innovation programme under grant agreement No. 950618 (STREAMLINE project).

Disclosures

The authors have no conflicts of interest to declare.

REFERENCES

[1] Alfano, R. R., [*The supercontinuum laser source: the ultimate white light*], Springer Nature (2023).

[2] Dudley, J. M. and Taylor, J. R., [*Supercontinuum generation in optical fibers*], Cambridge University Press (2010).

[3] Zorin, I., Su, R., Prylepa, A., Kilgus, J., Brandstetter, M., and Heise, B., "Mid-infrared fourier-domain optical coherence tomography with a pyroelectric linear array," *Opt. Express* **26**, 33428–33439 (Dec 2018).

[4] Petersen, C., Møller, U., Kubat, I., Zhou, B., Dupont, S., Ramsay, J., Benson, T., Sujecki, S., Abdel-Moneim, N., Tang, Z., Furniss, D., Seddon, A., and Bang, O., "Mid-infrared supercontinuum covering the 1.4–13.3 m molecular fingerprint region using ultra-high na chalcogenide step-index fibre," *Nature Photonics* **8**, 830–834 (2014).

[5] Manninen, A., Kääriäinen, T., Parviainen, T., Buchter, S., Heiliö, M., and Laurila, T., "Long distance active hyperspectral sensing using high-power near-infrared supercontinuum light source," *Opt. Express* **22**, 7172–7177 (Mar 2014).

[6] Poudel, C. and Kaminski, C. F., "Supercontinuum radiation in fluorescence microscopy and biomedical imaging applications," *J. Opt. Soc. Am. B* **36**, A139–A153 (Feb 2019).

[7] Udem, T., Holzwarth, R., and Haensch, T., "Optical frequency metrology," *Nature* **416**, 233–7 (04 2002).

[8] Lamb, E. S., Carlson, D. R., Hickstein, D. D., Stone, J. R., Diddams, S. A., and Papp, S. B., "Optical-frequency measurements with a Kerr microcomb and photonic-chip supercontinuum," *Phys. Rev. Appl.* **9**, 024030 (Feb 2018).

[9] Sylvestre, T., Genier, E., Ghosh, A. N., Bowen, P., Genty, G., Troles, J., Mussot, A., Peacock, A. C., Klimczak, M., Heidt, A. M., et al., "Recent advances in supercontinuum generation in specialty optical fibers," *JOSA.B* **38**(12), F90–F103 (2021).

[10] Oh, D. Y., Sell, D., Lee, H., Yang, K. Y., Diddams, S. A., and Vahala, K. J., "Supercontinuum generation in an on-chip silica waveguide," *Opt. Lett.* **39**, 1046–1048 (Feb 2014).

[11] Halir, R., Okawachi, Y., Levy, J. S., Foster, M. A., Lipson, M., and Gaeta, A. L., "Ultrabroadband supercontinuum generation in a cmos-compatible platform," *Opt. Lett.* **37**, 1685–1687 (May 2012).

[12] Johnson, A. R., Mayer, A. S., Klenner, A., Luke, K., Lamb, E. S., Lamont, M. R. E., Joshi, C., Okawachi, Y., Wise, F. W., Lipson, M., Keller, U., and Gaeta, A. L., "Octave-spanning coherent supercontinuum generation in a silicon nitride waveguide," *Opt. Lett.* **40**, 5117–5120 (Nov 2015).

[13] Lafforgue, C., Guerber, S., Ramírez, J. M., Marcaud, G., Alonso-Ramos, C., Xavier, L. R., Marris-Morini, D., Cassan, E., Baudot, C., Boeuf, F., Cremer, S., Monfray, S., and Vivien, L., "Broadband supercontinuum generation in nitrogen-rich silicon nitride waveguides using a 300 mm industrial platform," *Photonics Research* **8** (01 2020).

[14] Duchesne, D., Peccianti, M., Lamont, M. R. E., Ferrera, M., Razzari, L., Légaré, F., Morandotti, R., Chu, S., Little, B. E., and Moss, D. J., "Supercontinuum generation in a high index doped silica glass spiral waveguide," *Opt. Express* **18**, 923–930 (Jan 2010).

[15] Sinobad, M., Monat, C., Luther-Davies, B., Ma, P., Madden, S., Moss, D., Mitchell, A., Allioux, D., Orobtchouk, R., Boutami, S., Hartmann, J.-M., Fedeli, J.-M., and Grillet, C., "Mid-infrared octave spanning supercontinuum generation to 8.5 m in silicon-germanium waveguides," *Optica* **5** (03 2018).

[16] Montesinos-Ballester, M., Lafforgue, C., Frigerio, J., Ballabio, A., Vakarin, V., Liu, Q., Ramirez, J. M., Roux, X. L., Bouville, D., Barzaghi, A., Alonso-Ramos, C., Vivien, L., Isella, G., and Marris-Morini, D., "On-Chip Mid-Infrared Supercontinuum Generation from 3 to 13 μm Wavelength," *ACS photonics* **7**, 3423–3429 (Dec. 2020).

[17] Hammani, K., Markey, L., Lamy, M., Kibler, B., Arocas, J., Fatome, J., Dereux, A., Weeber, J.-C., and Finot, C., "Octave spanning supercontinuum in titanium dioxide waveguides," *Applied Sciences* **8** (04 2018).

[18] Lamont, M. R., Luther-Davies, B., Choi, D.-Y., Madden, S., and Eggleton, B. J., "Supercontinuum generation in dispersion engineered highly nonlinear ($\gamma = 10$ /w/m) as2s3 chalcogenide planar waveguide," *Opt. Express* **16**, 14938–14944 (Sep 2008).

[19] Li, C., Ren, X., Wu, H., Zheng, R., Zhao, J., Ouyang, D., Du, C., Yan, P., and Ruan, S., "Octave-spanning visible supercontinuum generation from an aluminum nitride single crystal pumped by a 355nm nanosecond pulse," *Chin. Opt. Lett.* **16**, 043201 (Apr 2018).

[20] Granger, G., Bailly, M., Delahaye, H., Jimenez, C., Tiliouine, I., Leventoux, Y., Orlianges, J., Couderc, V., Gérard, B., Becheker, R., Idlahcen, S., Godin, T., Hideur, A., Grisard, A., Lallier, E., and Février, S., "Gaas-chip-based mid-infrared supercontinuum generation," *Light: Science Applications* **12** (10 2023).

[21] Fiaboe, K. F., Torre, A. D., Mitchell, A., Monat, C., Grillet, C., and Nguyen, T., "Design of Mid-Infrared Supercontinuum Generation in a strip-loaded LNOI Waveguide through lateral leakage engineering," in [*European Conference on Integrated Optics*], (Apr. 2023).

[22] Brès, C.-S., Torre, A. D., Grassani, D., Brasch, V., Grillet, C., and Monat, C., "Supercontinuum in integrated photonics: generation, applications, challenges, and perspectives," *Nanophotonics* **12**(7), 1199–1244 (2023).

[23] Little, B., "A vlsi photonics platform," in [*Optical Fiber Communication Conference*], *Optical Fiber Communication Conference* , ThD1, Optica Publishing Group (2003).

[24] Zerbib, M., Hoang, V., Beugnot, J., Huy, K., Little, B., Chu, S., Moss, D., Morandotti, R., Wetzel, B., and Sylvestre, T., "Observation de la diffusion brillouin dans un guide d'ondes intégré de silice dopée à haut indice,"

[25] Webb, K. E., Xu, Y. Q., Erkintalo, M., and Murdoch, S. G., "Generalized dispersive wave emission in nonlinear fiber optics," *Opt. Lett.* **38**, 151–153 (Jan 2013).

[26] Agrawal, G. P., [*Nonlinear Fiber Optics, fifth edition*], Elsevier & Academic Press (2013).

[27] Li, G., Li, Y., Ye, F., Li, Q., Wang, S. H., Wetzel, B., Davidson, R., Little, B., and Chu, S. T., "Supercontinuum Generation in Dispersion Engineered Highly Doped Silica Glass Waveguides," *Laser and Photonics Reviews* **17**, 2200754 (Oct. 2023).

[28] Moss, D., Morandotti, R., Gaeta, A., and Lipson, M., "New cmos-compatible platforms based on silicon nitride and hydex for nonlinear optics," *Nature Photonics* **7**, 597–607 (07 2013).